nature structural & molecular biology

ARTICLES

https://doi.org/10.1038/s41594-018-0182-x

Nascent-protein ubiquitination is required for heat shock–induced gene downregulation in human cells

Fernando Aprile-Garcia[1,5], Parul Tomar[1,2,5], Barbara Hummel[1,2], Ashkan Khavaran[1,3] and Ritwick Sawarkar[1,4*]

Proteotoxic stress such as heat shock causes heat-shock factor (HSF)-dependent transcriptional upregulation of chaperones. Heat shock also leads to a rapid and reversible downregulation of many genes, a process we term stress-induced transcriptional attenuation (SITA). The mechanism underlying this conserved phenomenon is unknown. Here we report that enhanced recruitment of negative transcription elongation factors to gene promoters in human cell lines induces SITA. A chemical inhibitor screen showed that active translation and protein ubiquitination are required for the response. We further find that proteins translated during heat shock are subjected to ubiquitination and that p38 kinase signaling connects cytosolic translation with gene downregulation. Notably, brain samples of subjects with Huntington's disease also show transcriptional attenuation, which is recapitulated in cellular models of protein aggregation similar to heat shock. Thus our work identifies an HSF-independent mechanism that links nascent-protein ubiquitination to transcriptional downregulation during heat shock, with potential ramifications in neurodegenerative diseases.

When eukaryotic cells are exposed to environmental stress, they mount an adaptive, conserved and coordinated response at the levels of transcription, translation, cell cycle and metabolism. The transcriptional response called the heat-shock response is typified by upregulation of heat-shock proteins or chaperones driven by the transcription factor heat-shock factor (HSF)[1]. Initially identified using heat-shock stress, the conserved HSF-driven response is now known to be induced by a variety of cellular conditions[2]. Clinical studies have highlighted the relevance of the heat-shock response in cancer and neurodegeneration[3,4].

Early studies have shown that stress such as heat shock not only upregulates chaperone genes, but also causes transcriptional downregulation of a handful of genes tested[5,6]. Recent genome-wide technologies have confirmed a critical aspect of the heat-shock response: transcriptional downregulation of many highly expressed genes involved in metabolism, protein synthesis and cell cycle[7,8]. Stress-induced transcriptional attenuation (SITA) is a rapid process conserved across *Drosophila melanogaster*[9], mouse[7] and human cells[10]. By downregulating the transcription of key genes, cells probably shift their resources from growth-promoting anabolic activities to dealing with proteotoxic stress. Despite the importance and conserved nature of SITA, relatively little is known about its underlying mechanistic basis. Two key questions need to be addressed: first, how are the rapid and reversible changes in transcription achieved at a molecular level; and second, how is the stress of heat shock sensed and communicated to transcriptional effectors? The primary stress sensor for chaperone upregulation, HSF, is not required for SITA[7], suggesting an HSF-independent mechanism of stress sensing. How this mechanism is integrated with cellular stress response pathways is not understood.

Metazoan transcription proceeds through two highly regulated steps[11,12]. First, recruitment of RNA polymerase II (RNA Pol II) to core promoters leads to formation of a pre-initiation complex that transcribes about 20–60 bases downstream of transcription start sites (TSSs) and pauses. Sequence-specific transcription factors along with general transcription factors orchestrate this step. Second, release of promoter-proximal-paused RNA Pol II into productive elongation enables generation of a full-length transcript. Interplay between positive and negative transcription elongation factors (P-TEFs and N-TEFs, respectively) determines the fate of paused RNA Pol II, which is either termination followed by dissociation from promoters or transition to its elongating form. N-TEFs comprise several complexes including negative elongation factor (NELF), DRB-sensitivity inducing factor (DSIF), Integrator, tripartite motif containing 28 (TRIM28) and polymerase-associated factor 1 (PAF1)[13–16]. N-TEFs oppose the elongation activity of P-TEFb, which consists of cyclin-dependent kinase 9 (Cdk9) and cyclin T[17]. How stress affects the activity of RNA Pol II regulatory factors to control rapid transcriptional downregulation remains unknown. This study aims to understand the molecular mechanism underlying SITA using heat shock as a stress model. Specifically, we address critical questions regarding sensors and transcriptional effectors that orchestrate SITA.

Results

Heat shock causes enrichment of N-TEFs at chromatin. We quantified genome-wide transcription by precision run-on sequencing (PRO-seq)[18] and RNA Pol II chromatin immunoprecipitation sequencing (ChIP-seq) to confirm SITA in human cells. Of ~6,500 genes analyzed by PRO-seq and RNA Pol II ChIP-seq, 3,625 and 2,000 genes were downregulated upon heat shock in HEK293 and K562

[1]Max Planck Institute of Immunobiology and Epigenetics, Freiburg, Germany. [2]Faculty of Biology, University of Freiburg, Freiburg, Germany. [3]Faculty of Medicine, University of Freiburg, Freiburg, Germany. [4]CIBSS, Centre for Integrative Biological Signalling Studies, University of Freiburg, Freiburg, Germany. [5]These authors contributed equally: F. Aprile-Garcia, P. Tomar. *e-mail: sawarkar@ie-freiburg.mpg.de

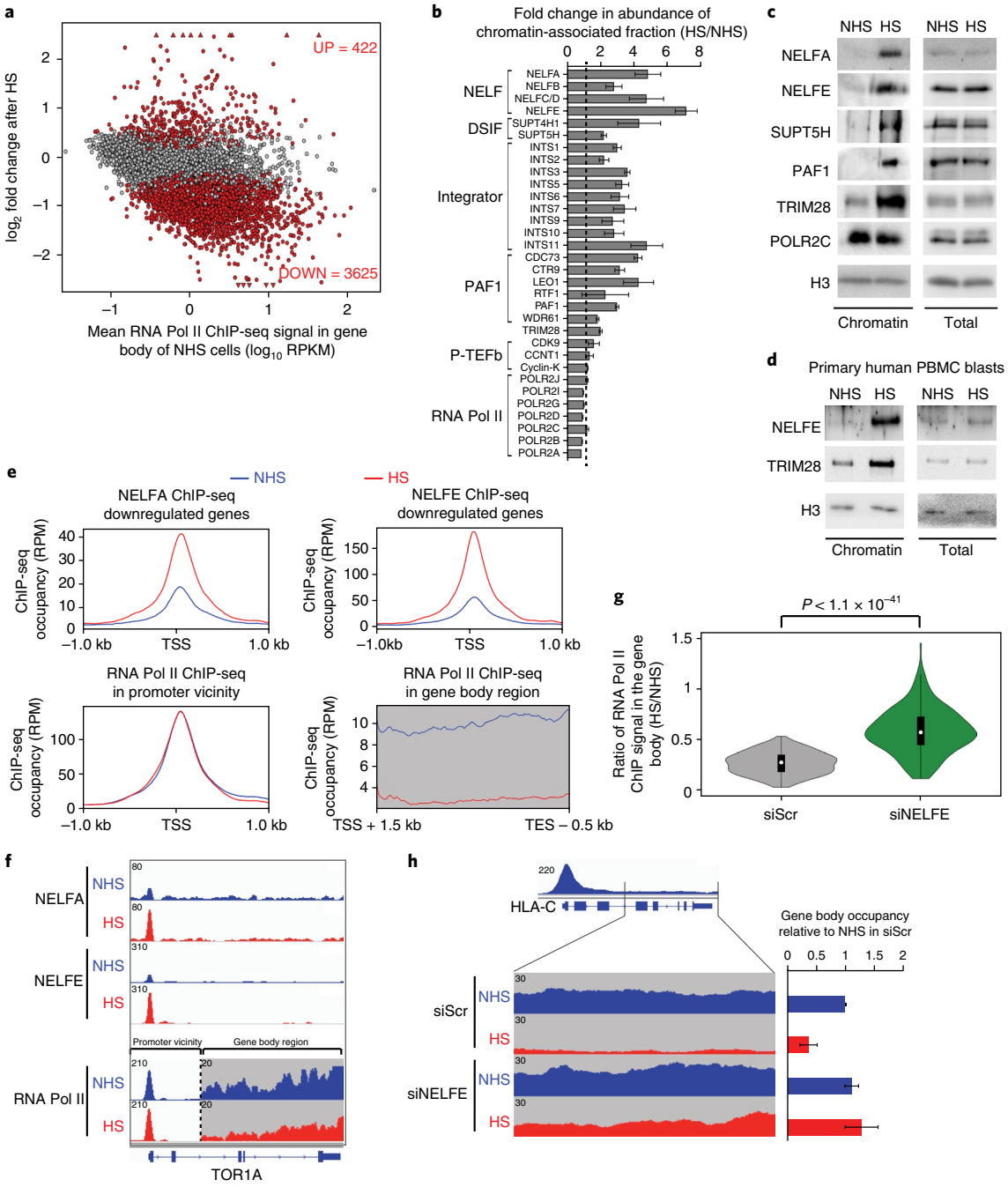

Fig. 1 | N-TEFs are enriched at chromatin upon heat shock. a, Change in RNA Pol II gene body occupancy measured by ChIP-seq in heat-shocked (HS) compared to non-heat-shocked (NHS) HEK293 cells plotted against average RNA Pol II occupancy in gene bodies. Genes with significant (red dots) or nonsignificant (gray dots) changes in gene-body RNA Pol II occupancy are indicated ($P < 0.01$ based on DESeq2 analysis, $n = 5$ independent experiments). UP, significantly upregulated genes; DOWN, significantly downregulated genes. RPKM, reads per kilobase per million fragments mapped. **b**, Mean fold changes in abundance of chromatin-associated N-TEFs (subunits of NELF, DSIF, Integrator and PAF1 complexes and TRIM28), P-TEFb and RNA Pol II upon heat shock. Error bars represent s.e.m. ($n = 3$ biologically independent cell cultures). **c**,**d**, Western blot analysis of total cell extract and chromatin fractions from HEK293 cells (**c**) and primary T cell blasts (**d**). **e**, Metaplots of NELFA, NELFE and RNA Pol II binding around TSSs of downregulated genes in K562 cells. Lower right (gray), metaplot of RNA Pol II occupancy in gene bodies (TSS + 1.5 kb to TES – 0.5 kb). List of genes used for analyses in Fig. 1e is available in Supplementary Data Set 2. **f**, Top, genome browser tracks showing ChIP-seq occupancy of indicated proteins in K562 cells. Bottom, RNA Pol II occupancy in gene body regions shown at a scale different than for promoter region. Vertical scale indicates normalized read density in RPM. **g**, Effect of NELFE depletion on RNA Pol II ChIP-seq occupancy in gene bodies is shown as a violin plot. The plot depicts density distribution of data comprising 245 genes (see Supplementary Data Set 1), with white dot, black bar and thin black line indicating median, interquartile range and 95%-confidence interval, respectively. siNELFE, siRNA against NELFE; siScr, scrambled siRNA. *P* value from Wilcoxon test is indicated. **h**, Genome browser tracks showing RNA Pol II ChIP-seq occupancy. Right, Gene body RNA Pol II occupancy as mean normalized read density with s.e.m. ($n = 2$ independent experiments). Uncropped blots are in Supplementary Data Set 5.

cells, respectively (Fig. 1a, Supplementary Fig. 1 and Supplementary Data Sets 1–3). Using primers that recognize unspliced nascent transcripts in a quantitative PCR assay[19] (Supplementary Fig. 2a,b), we confirmed that heat shock–induced decrease in RNA Pol II within a gene body corresponds to reduction in nascent-transcript synthesis in various human cell lines (Supplementary Fig. 2c) as well as in primary human T cell blasts derived from peripheral blood mononuclear cells (PBMCs) (Supplementary Fig. 2d).

To identify transcriptional effectors that enable SITA, we quantified heat shock–induced changes in the chromatin proteome by stable isotope labeling with amino acids in cell cultures (SILAC) followed by mass spectrometry[20]. Several proteins showed an increased abundance at chromatin upon heat shock (Supplementary Data Set 4). We searched for gene regulatory complexes whose members showed an increase at chromatin in the SILAC data in an unbiased manner (see Methods). The NELF complex was the highest ranked regulatory complex enriched at chromatin ($P = 9.48 \times 10^{-5}$, See Methods), with all its protein members showing significant enrichment (Supplementary Table 1 and Fig. 1b). We observed that heat shock caused a two- to seven-fold increase in the chromatin-associated fraction of several known N-TEF protein complexes beyond NELF, namely DSIF, Integrator, PAF1 and TRIM28 (Fig. 1b and Supplementary Data Set 4). Using immunoblots in different human cell lines, we validated the increased chromatin association of NELFA and NELFE of the NELF complex, as well as SUPT5H of the DSIF complex, PAF1 and TRIM28 (Fig. 1c and Supplementary Fig. 3a). There was no change in total cellular levels of N-TEFs proteins (Fig. 1c, Supplementary Fig. 3a and Supplementary Data Set 5), suggesting that heat shock causes an increase in chromatin association of the available cellular pool of N-TEFs. We also found that heat shock causes very little change in the chromatin abundance of RNA Pol II subunits and the P-TEFb complex, comprising Cdk9 and cyclin T subunits (Fig. 1b,c). The increased chromatin association was also observed in primary human cells exposed to heat shock (Fig. 1d), indicating that this observation is not restricted to cell lines. The enhanced chromatin binding of N-TEFs was observed using two different heat-shock regimes (Supplementary Fig. 3b) and employing distinct biochemical procedures to extract chromatin (Supplementary Fig. 3c–e). Thus we conclude that exposure of human cells to heat shock leads to an increase in chromatin association of N-TEFs.

To identify the genomic binding sites occupied by N-TEFs in non-heat-shocked and heat-shocked cells, we performed ChIP-seq of NELFA and NELFE. The data revealed that heat shock causes an increase of NELFA and NELFE at promoters of SITA target genes (Fig. 1e,f). Some 77% and 92% of downregulated genes showed an increase of NELFA and NELFE, respectively, at their promoters (Supplementary Fig. 3f and Fig. 1f), but not at SITA nontarget genes that did not change their expression levels (Supplementary Fig. 3g and Supplementary Data Set 6). We also analyzed RNA Pol II ChIP-seq data to study RNA Pol II dynamics at genes showing SITA. As we expected for downregulated genes, there was a marked decrease in the amount of RNA Pol II in gene bodies, confirming a reduction in the elongating form of RNA Pol II (Fig. 1e,f and Supplementary Fig. 1a–c,f,g). Some 50% of downregulated genes showed at least 40% reduction in the amount of RNA Pol II in gene bodies (Supplementary Fig. 1g). However, heat shock did not change promoter-proximal binding of Pol II at genes where NELFA and NELFE showed an increase in ChIP signal (Fig. 1e,f). Thus heat shock causes a reduction in the release of promoter-proximal RNA Pol II into elongation mode, in line with recent reports[7].

To test the function of N-TEFs as transcriptional effectors[21] of SITA, we exposed NELFE-depleted cells to heat shock and assessed transcription by RNA Pol II ChIP-seq. Heat shock caused robust transcriptional downregulation of SITA target genes in cells treated with scrambled short interfering RNA (siRNA) (Fig. 1g,h). However, NELFE knockdown significantly affected the ability of cells to downregulate SITA targets, with little effect on control genes (Fig. 1g,h, Supplementary Fig. 3g,h and Supplementary Data Set 7). NELFE- and PAF1-depleted cells did not efficiently downregulate nascent-transcript levels of tested genes upon heat shock (Supplementary Fig. 3i), in line with a recent study on PAF1 (ref. [22]). Thus our data combining proteomic and genomic approaches suggest that increased abundance of N-TEFs at chromatin upon heat shock is required for SITA in human cells.

Metabolic change as a phenotypic consequence of SITA. SITA-target genes were enriched for the gene ontology term "metabolism." We tested whether transcriptional downregulation of key metabolic genes by the NELF-based mechanism described above contributes to metabolic changes seen upon heat shock. We focused on the "lower glycolysis" pathway and lactate formation during central carbon metabolism (Supplementary Fig. 4a)[23]. Genes encoding five of six enzymes in the pathway were transcriptionally downregulated during heat shock in a NELFE-dependent manner (Supplementary Fig. 4b,c). We quantified intermediary metabolites in this pathway as a phenotypic readout of SITA. Our assay using a mass spectrometry–based approach allowed us to measure three metabolites in this pathway: phosphoglycerate (a combination of 2- and 3-phosphoglycerate), phosphoenol-pyruvate and lactate. We found that the abundance of all three metabolites was reduced upon heat shock (Supplementary Fig. 4d), in line with reduction in transcription of the responsible enzymes (Supplementary Fig. 4b,c). Moreover, a stress-mediated decrease in metabolite abundance was significantly reversed in NELFE-knockdown cells (Supplementary Fig. 4d). These results emphasize the importance of NELFE-dependent SITA in contributing to stress-induced metabolic changes.

Active translation is required for SITA. How is the stress of heat shock sensed to modulate N-TEF recruitment to chromatin and enable SITA? HSF transduces the signal of heat shock to chaperone transcription[2]. Knockdown, knockout or pharmacological inhibition of HSF in independent experiments had no effect on the increase of N-TEFs at chromatin and SITA (Fig. 2a and Supplementary Fig. 5a–f), in line with recent studies in flies and mouse cells[7,9].

To identify mechanisms responsible for SITA, we conducted a low-throughput chemical inhibitor screen in HEK293 cells and used increased NELFE recruitment to chromatin as a readout. The screen identified two chemicals that blocked the increased abundance of NELFE at chromatin during heat shock: cycloheximide, an inhibitor of protein translation, and NSC 624206 (ref. [24]), an inhibitor of ubiquitin E1 ligase (Ub-E1) (Supplementary Fig. 5g). We confirmed the results of the screen, first focusing on protein translation using cycloheximide and puromycin in cell lines (Fig. 2b), and in primary human cells (Fig. 2c). Translation inhibition blocked the increase of NELFA binding to promoters of SITA-target genes (Fig. 2d and Source Data). Notably, the short duration of treatment with translation inhibitors used in the experiments did not change the total cellular levels of N-TEFs (Fig. 2b,c). This rules out the possibility that only newly synthesized N-TEFs are recruited to chromatin during heat shock. As we expected, acute exposure to cycloheximide abrogated protein synthesis (Supplementary Fig. 5h,i) and heat shock–induced chaperone transcription (Supplementary Fig. 5j)[25].

Translation inhibition during heat shock also affected transcriptional downregulation caused by heat shock. Cycloheximide-treated cells did not downregulate nascent transcription at tested loci (Supplementary Fig. 5k). Genome-wide studies using RNA Pol II ChIP-seq confirmed that cycloheximide treatment significantly affected SITA (Fig. 2e,f). Cycloheximide treatment for the short duration used in the experiments did not affect transcription on its own (Fig. 2f and Supplementary Fig. 5l). This observation suggests that translation defects per se do not cause

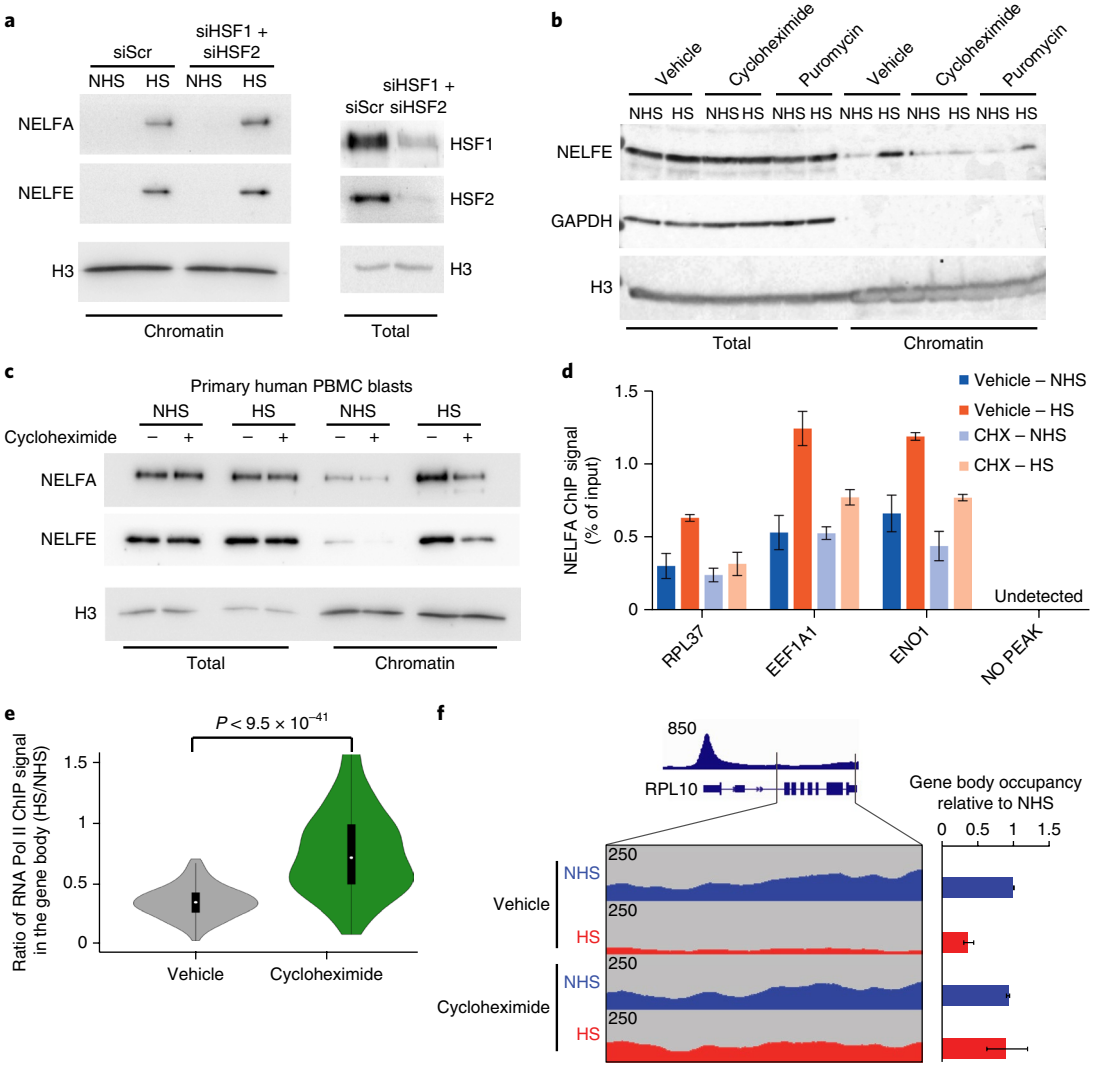

Fig. 2 | Active translation is required for stress-induced increase of N-TEFs at chromatin and SITA. a,**b**, Western blot analyses of indicated proteins in chromatin fraction or total cell extracts of HEK293 cells. H3, histone H3; GAPDH, loading and fractionation controls. **c**, Western blot analyses of NELFA and NELFE in total cell extracts and chromatin fractions of primary T cell blasts derived from human PBMCs with or without heat shock, treated with vehicle (–) or cycloheximide (+). Histone H3 was used as loading control. **d**, ChIP-qPCR measuring NELFA occupancy at indicated gene promoters in HS and NHS K562 cells treated with vehicle or cycloheximide (CHX). "No peak" primer set amplifies a genomic region not expected to bind NELFA and acts as a negative control. The *y*-axis indicates the mean amount of immunoprecipitated DNA relative to starting input material. Error bars represent s.e.m. ($n = 2$ independent experiments). **e**, Effect of cycloheximide on RNA Pol II ChIP-seq occupancy in gene bodies is shown as a violin plot. The plot depicts density distribution of data comprising 245 genes (see Supplementary Data Set 1), with white dot, black bar and thin black line indicating the median, interquartile range and 95% confidence interval, respectively. Statistical significance determined by Wilcoxon test is indicated as *P*. **f**, Representative genome browser tracks showing RNA Pol II ChIP-seq occupancy at the *RPL10* gene body in vehicle- and cycloheximide-treated NHS and HS cells. Right, quantification of gene body RNA Pol II occupancy as mean normalized read density. $n = 2$ independent experiments, error bars depict s.e.m. Uncropped blots are in Supplementary Data Set 5. Source data for **d** are available in Source Data.

transcriptional attenuation. Thus our observations suggest that active translation is necessary for heat shock–induced increase of N-TEFs at chromatin and SITA.

Protein ubiquitination is required for SITA. We found that Ub-E1 ligase inhibitor decreased heat shock–induced N-TEF recruitment to chromatin in a manner similar to translation inhibition (Supplementary Fig. 5g). Heat shock increased K48-linked polyubiquitination in several independent cell lines (Supplementary Fig. 6a and ref. [26]). Translation inhibition substantially decreased heat shock–induced protein ubiquitination (Fig. 3a, Supplementary Fig. 6b and ref. [27]), suggesting that protein translation and ubiquitination may work together to regulate SITA. We tested whether heat shock–induced protein ubiquitination was required for SITA. An acute 30-min treatment of cells with the Ub-E1 inhibitor NSC 624206 reduced polyubiquitination during heat shock as we expected (Fig. 3b). Ub-E1 inhibition also reduced the recruitment of NELFA and NELFE to chromatin in heat-shocked cells (Fig. 3b), confirming our results from the screen (Supplementary Fig. 5g). Importantly, cells treated with Ub-E1 inhibitor showed impairment in their ability to downregulate transcription upon heat shock, as determined by nascent-transcript quantitative PCR (qPCR) assay (Fig. 3c) and by RNA Pol II ChIP-seq (Fig. 3d,e). Notably, the decrease in polyubiquitination upon Ub-E1 inhibition was not as strong as seen with cycloheximide (Fig. 3a,b), owing to the low concentration of Ub-E1 inhibitor used in the study to avoid toxicity and a direct effect on

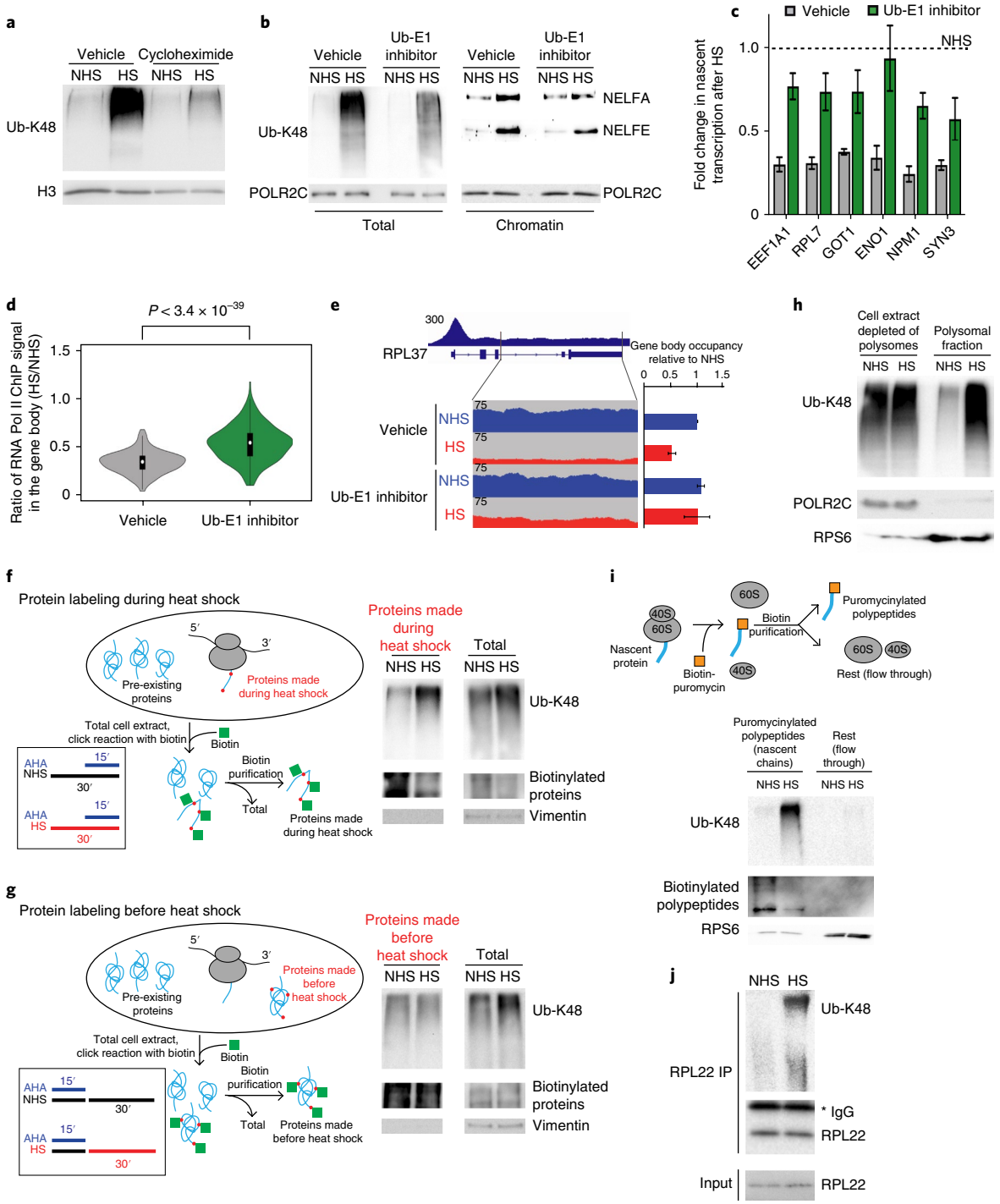

Fig. 3 | Ubiquitination of nascent proteins is required for SITA. a,**b**, Western blot analysis of HEK293 total cell extracts and chromatin fractions using indicated antibodies. Histone H3 and POLR2C, loading controls. **c**, RT-qPCR-based nascent-transcript quantification of indicated genes in HEK293 cells. Mean levels with s.e.m. are shown ($n = 3$ independent experiments). **d**, Effect of Ub-E1 inhibitor on RNA Pol II ChIP-seq occupancy in gene bodies is shown as a violin plot. The plot depicts density distribution of data comprising 245 genes (see Supplementary Data Set 1), with white dot, black bar and thin black line indicating median, interquartile range and 95% confidence interval, respectively. *P* from Wilcoxon test is indicated. **e**, Genome browser tracks showing RNA Pol II ChIP-seq occupancy. Right, gene body RNA Pol II occupancy as mean normalized read density with s.e.m. ($n = 2$ independent experiments). **f**, Left, experimental workflow for labeling and purification of proteins synthesized during the last 15 min of a 30 min heat shock. Right, western blot analysis of K48-linked protein ubiquitination of HEK293 samples as indicated. AHA, L-azidohomoalanine, a methionine analog for click reaction. **g**, Left, experimental workflow for labeling and purification of proteins made before heat shock. Right, western blot analysis of K48-linked protein ubiquitination of HEK293 samples as indicated. In **f**,**g**, vimentin and biotinylated proteins were used as loading control. **h**, Western blot analysis of K48-linked protein ubiquitination in fractions obtained after sucrose cushion sedimentation. Polysomal fraction and the corresponding supernatant depleted of polysomes are shown (see Methods for details). POLR2C and RPS6 were used as loading and purity controls. **i**, In vitro puromycinylation was used to label ribosome-associated nascent chains with biotin tags. Top, diagram depicting isolation of puromycinylated proteins. Bottom, western blot analysis using indicated antibodies. RPS6, loading control. **j**, Immunoblot using indicated antibodies in input or RPL22 immunoprecipitates (IP) from HEK293 cells. Ub-K48, anti-ubiquitin antibody, lysine 48-specific.*, nonspecific band. Uncropped blots are in Supplementary Data Set 5. Source data for **c** are available in Source Data.

transcription (Supplementary Fig. 6c). Consequently, the effect of Ub-E1 inhibition on NELF recruitment to chromatin is also weaker than that of cycloheximide (Figs. 2b and 3b). Thus our results implicate protein ubiquitination in the regulation of SITA.

The effect of inhibitors of translation and Ub-E1 on SITA could also be explained by various indirect possibilities, such as a decrease in ubiquitin levels, as previously reported for cycloheximide in yeast[28]. To address this point, we measured free ubiquitin levels after cycloheximide and Ub-E1 inhibitor treatment and detected no change in control or heat-shocked cells (Supplementary Fig. 6d,e). Another possibility is that Ub-E1 inhibitor affects the basal translation rate, thus mimicking cycloheximide and indirectly regulating SITA. However, Ub-E1 inhibition did not alter translation rates (Supplementary Fig. 6f). Thus protein ubiquitination per se can be directly implicated in SITA.

We next compared the kinetics of protein ubiquitination and transcriptional changes in the acute heat-shock model of HeLa cells[29]. We observed an increase of protein ubiquitination at 5 min of heat shock, the earliest time point we studied (Supplementary Fig. 7a). Transcriptional downregulation occurred gradually at around 10–15 min, reaching its peak at 60 min of heat shock (Supplementary Fig. 7b–d). In longer-term experiments, ubiquitination levels were lower at 4 h of heat shock than at 1 h of heat shock; these levels still remained much higher than in non-heat-shocked cells (Supplementary Fig. 7c). SITA target genes were still downregulated with increased N-TEFs at chromatin at 4 h of heat shock (Supplementary Fig. 7d–f). Thus even as cells adapt to stress by decreasing chaperone transcription at longer time points (Supplementary Fig. 7e and ref. [29]), SITA continues to be maintained. Thus, protein ubiquitination temporally precedes the onset of transcriptional attenuation caused by heat shock, suggesting that the process of protein ubiquitination may serve as a trigger for SITA.

Nascent proteins are ubiquitinated upon heat shock. The observation that translation inhibition reduces heat shock–induced protein ubiquitination raises the possibility that proteins translated during heat shock get ubiquitinated themselves. We tested this possibility by selectively labeling proteins translated during heat shock and subsequently purifying them from total cell extracts (Fig. 3f). We focused on the initial 30 min of heat shock, when general translation has not been completely repressed (Fig. 3f). We found that heat shock caused a robust increase in the ubiquitination of proteins translated during heat shock (Fig. 3f). Notably, proteins synthesized just before heat shock did not show any change in ubiquitination levels (Fig. 3g). Moreover, polysome isolation by sucrose cushion sedimentation[30] confirmed that heat shock–induced polyubiquitination is associated with the polysome fraction after 30 min of heat shock (Fig. 3h). We then performed biotin-puromycin labeling[31] on isolated polysomes to determine whether nascent chains were themselves ubiquitinated. Biotin-puromycin was incorporated in the nascent chain on the ribosome and puromycinylated chains were released from the ribosome (Fig. 3i). Puromycinylated nascent chains thus obtained from polysomes of heat-shocked cells showed increased ubiquitination as compared to those of non-heat-shocked cells. Importantly, the flow-through fraction containing non-nascent proteins did not show any increase in ubiquitination upon heat shock (Fig. 3i). Therefore, the increase in ubiquitination of nascent chains quantitatively accounts for the total cellular increase in ubiquitination during 30 min of heat shock (Fig. 3i). We further validated the association of heat shock–induced polyubiquitinated proteins and ribosomes by performing immunoprecipitation of ribosomal subunit RPL22 (Fig. 3j). Thus, using four independent approaches, we demonstrate that nascent proteins are ubiquitinated upon heat shock with no ubiquitination of pre-existing proteins synthesized before the stress.

Cytosolic p38α kinase relocates to chromatin upon heat-shock. How does nascent-protein ubiquitination in the cytosol regulate N-TEFs at chromatin? We looked for stress-activated protein kinases[32–35] in the list of proteins that showed heat shock–induced increase in chromatin abundance (Fig. 1b and Supplementary Data Set 4). To our surprise, the only stress-activated protein kinase enriched at chromatin after heat shock was p38α kinase (MAPK14); it was enriched up to levels comparable to those of N-TEFs (Fig. 4a,b, compare enrichment levels with Fig. 1b). p38 is activated by heat shock[36]. The relocalization of MAPK14 from cytosol to chromatin depends on its catalytic activity, because a selective inhibitor of p38 kinase activity[37] SB203580, abrogated the relocalization (Supplementary Fig. 8a). Notably, inhibition of translation decreased the levels of chromatin-bound MAPK14 upon heat shock (Fig. 4c), suggesting that the activation and relocalization of MAPK14 to chromatin is controlled by upstream events involving nascent translation. ChIP-seq of MAPK14 revealed that heat shock causes an increase in MAPK14 at promoters of downregulated genes, paralleling the increase in N-TEFs at these SITA target promoters (Fig. 4d,e). There was no increase in MAPK14 at genes that do not change their expression levels upon heat shock (control genes), which also did not show an increase of N-TEFs (Fig. 4d). Upon MAPK14 inhibition, the heat shock–dependent enrichment of N-TEFs at chromatin was reduced (Fig. 4f), affecting SITA, as seen in a nascent-transcript qPCR assay, and globally altering RNA Pol II elongation, as assessed by ChIP-seq (Fig. 4g and Supplementary Fig. 8b,c). MAPK14 inhibition did not affect the RNA Pol II profile under basal conditions (Supplementary Fig. 8b,c), confirming the stress-specific function of this kinase in regulating transcription. Thus MAPK14 exhibits the three core tenets of a signaling pathway linking cytosolic events with nuclear gene regulation: first, MAPK14 is activated by heat shock and translocates to chromatin from the cytosol in a cycloheximide-sensitive manner. Second, the kinase is recruited to downregulated SITA promoters, providing target specificity to transcriptional effects of stress. Third, MAPK14 inhibition abrogates N-TEF recruitment to chromatin upon stress and consequent changes in RNA Pol II activity.

SITA beyond heat shock stress. Our results so far suggest that heat shock causes nascent-protein ubiquitination, MAPK14 activation and an increase in N-TEFs at chromatin leading to the transcriptional downregulation program called SITA. To characterize the breadth of SITA in cellular contexts beyond the heat-shock model of stress, we tested an acute source of protein misfolding. Arginine analog L-canavanine is incorporated in nascent polypeptides, but such polypeptides do not fold properly owing to chemical differences between arginine and canavanine[38]. As we expected, exposure of cells to canavanine caused an increase in protein ubiquitination (Fig. 5a, left). Proteins synthesized during canavanine treatment were specifically ubiquitinated without affecting the ubiquitination of proteins synthesized before canavanine addition (Fig. 5a). We observed increased ubiquitination of nascent chains in canavanine-treated cells compared to controls in biotin-puromycin experiments (Fig. 5b); this was reminiscent of heat shock–induced nascent-protein ubiquitination (Fig. 3i). Importantly, canavanine exposure caused an increase of NELFE binding to promoters of SITA-target genes as shown by ChIP (Fig. 5c), and downregulation of several SITA-target genes as shown by nascent-transcript qPCR assay (Fig. 5d). Canavanine treatment itself did not change free ubiquitin levels or translation rate (Supplementary Fig. 9a,b), ruling out indirect transcriptional consequences of exposure to canavanine. Thus features of SITA, namely nascent-protein ubiquitination, N-TEF recruitment to chromatin and transcriptional downregulation were evoked by inducing nascent chain misfolding in the absence of any temperature change. The results obtained using canavanine-induced protein misfolding further support the conclusion that the primary cause of heat

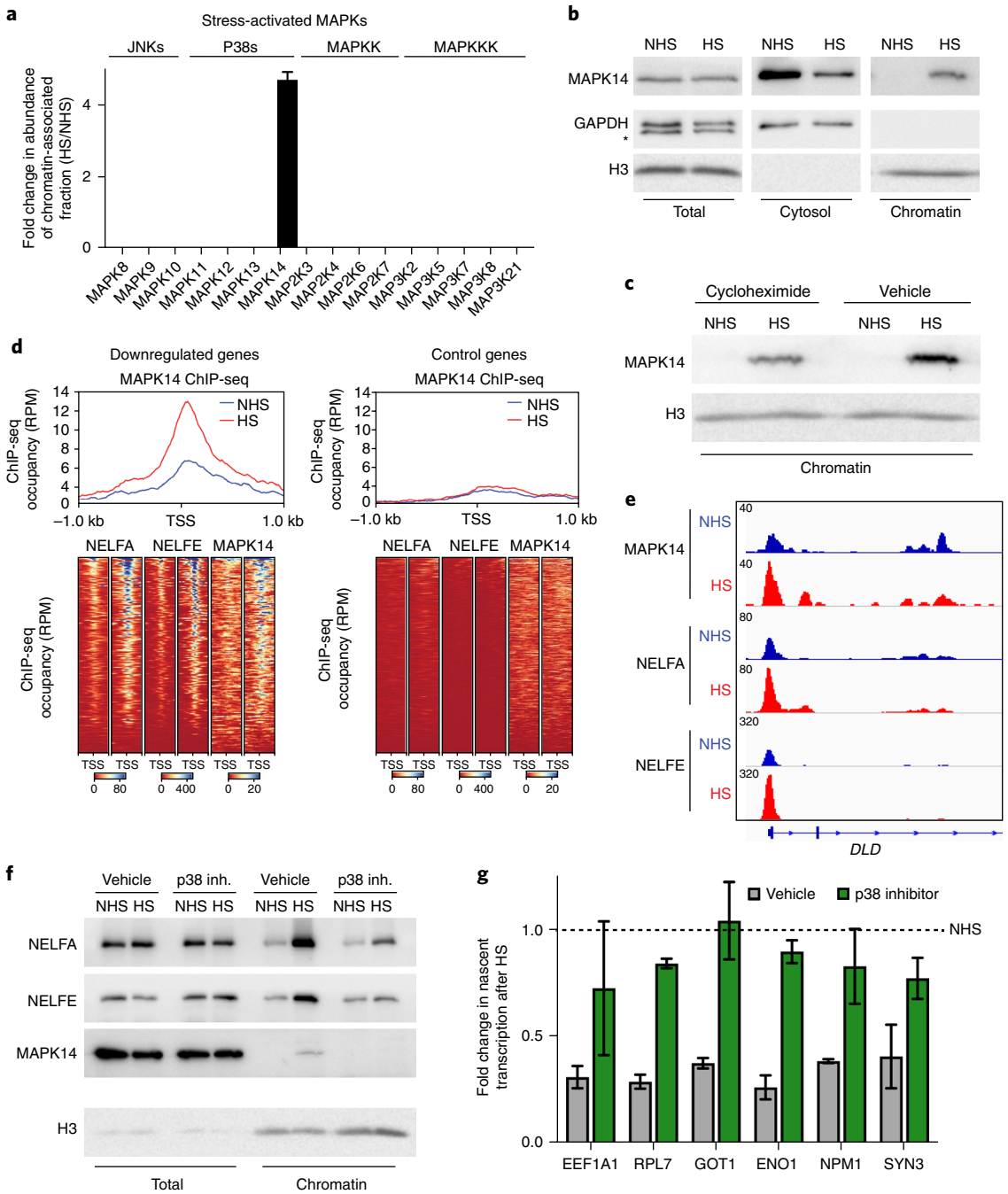

Fig. 4 | p38α kinase (MAPK14)-mediated signaling is required for SITA. a, Mean fold changes in abundance of chromatin-associated fraction of stress-activated MAPKs (JNK and p38 family kinases, and known MAPKK and MAPKKK of these pathways) were measured by quantitative SILAC in NHS and HS HEK293 cells. Error bars represent s.e.m. ($n = 3$ independent experiments). **b**, Western blot analysis of MAPK14 in total cell extract, cytosol and chromatin fractions from HEK293 cells with or without heat shock. GAPDH and histone H3 were used as loading control and to indicate the purity of the fractions. *, nonspecific band. **c**, Western blot analyses of MAPK14 in chromatin fractions of HEK293 cells with or without heat shock treated with cycloheximide or vehicle. Histone H3 was used as loading control. **d**, MAPK14 ChIP-seq analysis. Top, metaplots of MAPK14 binding around TSSs of 200 downregulated (left) and 416 control (right) genes in K562 cells with or without heat shock. *y*-axes indicate normalized ChIP-seq occupancy in RPM. Bottom, heatmaps of the occupancy of NELFA, NELFE and MAPK14 at the promoters of the top-downregulated genes (left) and control genes (right). Color-scaled intensities are in units of RPM. Genes used for analyses are available in Supplementary Data Sets 2 and 6. **e**, Genome browser tracks of a representative gene, *DLD*, showing ChIP-seq occupancy of MAPK14, NELFA and NELFE in K562 cells with or without heat shock. Vertical scale indicates normalized read density in RPM. **f**, Western blot analyses of NELFA, NELFE and MAPK14 in total cell extracts and chromatin fractions of K562 cells with or without heat shock treated with p38 inhibitor (p38 inh., SB203580) or vehicle. Histone H3 was used as loading control. **g**, RT-qPCR-based nascent-transcript quantification in HEK293 shown as mean; error bars, s.e.m. ($n = 2$ independent experiments). Uncropped blots are in Supplementary Data Set 5. Source data for **g** are available in Source Data.

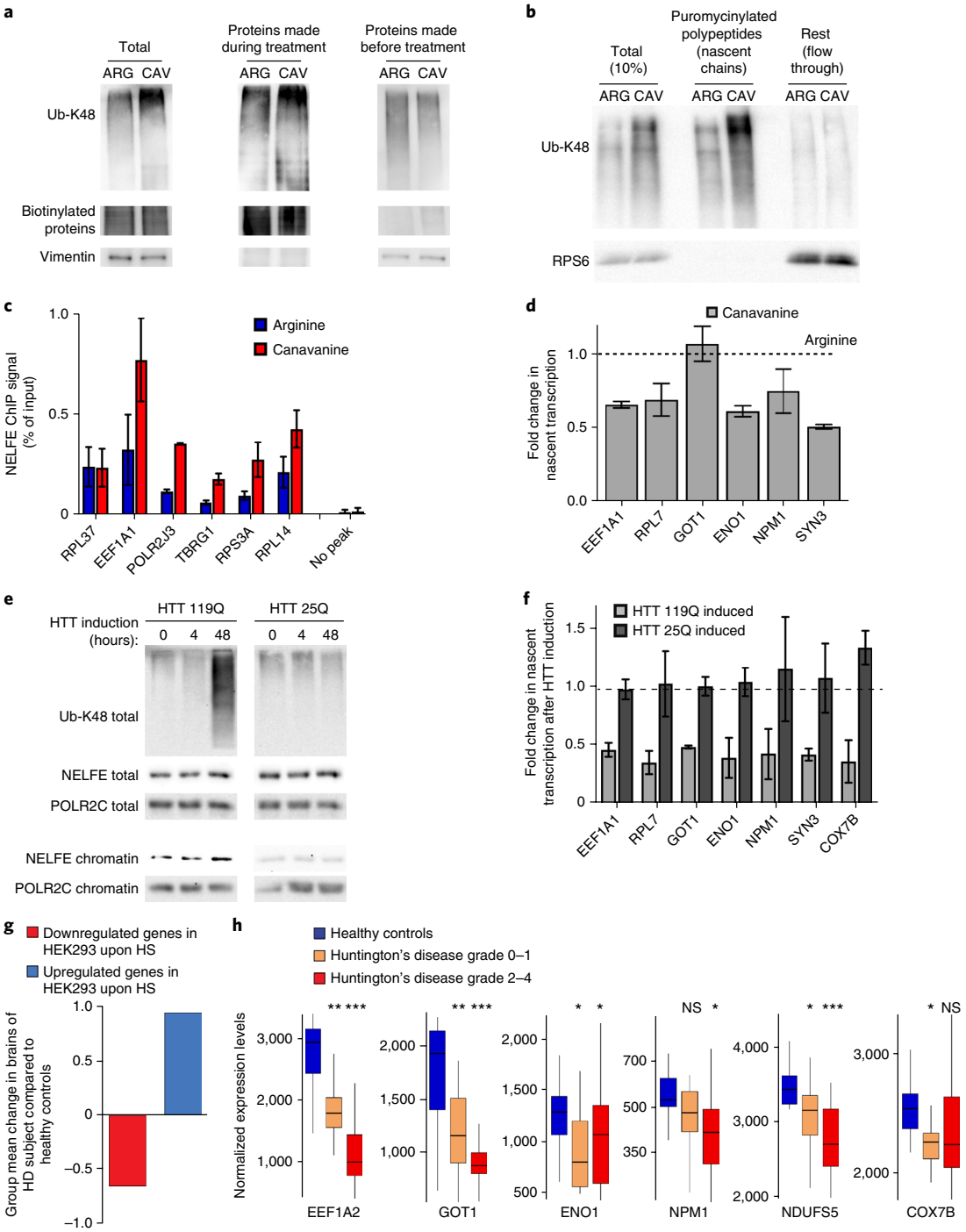

Fig. 5 | Acute and chronic proteotoxic stress cause gene downregulation. a,**b**, Western blot analyses of HEK293 cells after incubation for 2 h with L-arginine (ARG) or its analog L-canavanine (CAV). **a**, HEK293 fractions obtained as shown in Fig. 3f,g. Vimentin and biotinylated proteins were used as loading controls. **b**, In vitro puromycinylation reactions on polysomal fractions from HEK293 cells (obtained as shown in Fig. 3i). RPS6, loading control. **c**, ChIP-qPCR measuring mean NELFE occupancy at indicated gene promoters in HEK293 cells; error bars, s.e.m. ($n = 2$ independent experiments). "No peak" primer set amplifies genomic region not expected to bind NELFE and acts as a negative control. **d**, Mean fold change in nascent-transcript levels in HEK293 cells incubated with canavanine are shown with s.e.m. ($n = 2$ independent experiments). Nascent-transcript levels in HEK293 cells incubated with arginine were used as control to calculate fold change by qRT-PCR. **e**, Western blot analyses using indicated antibodies in total cell extracts and chromatin fractions of HEK293 expressing HTT variants upon induction for 0, 4 or 48 h. POLR2C, loading control. **f**, Mean fold change in nascent-transcript levels in HEK293 cells expressing HTT variants are shown; error bars, s.e.m. ($n = 3$ independent experiments). Uninduced control cells were used to calculate fold change in nascent transcription by qRT-PCR. **g**, Gene set analysis of expression data in brain samples of healthy controls and subjects with Huntington's disease. Gene sets were derived from HEK293 heat-shock analysis as indicated. **h**, Normalized expression levels of indicated genes in brain samples of healthy controls in comparison with Huntington's disease subjects. Box plots display the 25th and 75th percentile within the box with the median shown as a line. Whiskers show the interquartile range. Data taken from ref. [41]: shown are 32 controls, 16 subjects in disease grade 0–1 and 22 subjects in disease grade 2–4. Statistical significance determined by Student's *t*-test against healthy controls is indicated by asterisks. $^{*}P < 0.05$; $^{**}P < 5 \times 10^{-4}$ and $^{***}P < 5 \times 10^{-6}$. Uncropped blots are in Supplementary Data Set 5. Source data for **c**,**f** are in Source Data.

shock–mediated transcriptional downregulation is not increased temperature per se, but nascent-protein misfolding and ubiquitination. As an independent control, we implemented proteasome inhibitors that increase general protein ubiquitination without inducing co-translational misfolding. Treatment of cells with bortezomib, a specific inhibitor of proteasome, did not cause an increase of NELFE at chromatin or transcriptional downregulation (Supplementary Fig. 9c–e). Thus we conclude that nascent-protein ubiquitination, but not general proteotoxic stress, is responsible for SITA.

We next explored the possibility that disease-associated protein misfolding may also lead to transcriptional attenuation, similarly to canavanine-induced misfolding. Huntington's disease is an inheritable syndrome caused by misfolding of a single protein, Huntingtin (HTT). Ectopic expression of exon 1 of HTT protein with long polyglutamine tract (HTT 119Q) forms visible aggregates as compared to nonpathogenic HTT 25Q, which forms soluble protein (Supplementary Fig. 10a,b and ref. [39]). HTT aggregation caused an increase in K48-linked ubiquitination of proteins made during HTT expression (Fig. 5e and Supplementary Fig. 10c,d), correlating with an increase of NELFE levels at chromatin (Fig. 5e and Supplementary Fig. 10c,e). As we expected, the quantitative effect of NELFE increase at chromatin was more severe in the case of acute heat shock as compared to the chronic stress of misfolding of one protein. Nonetheless, ectopic expression of HTT 119Q, but not HTT 25Q, caused a reduction in nascent-transcript levels in independent cellular models including neuronal cell line SH-SY5Y (Fig. 5f and Supplementary Fig. 10a,b). Again, features of SITA, namely N-TEF recruitment to chromatin and transcriptional downregulation, were evoked by chronic protein misfolding without any temperature change. The occurrence of nascent-protein ubiquitination and p38 activation during HTT-induced SITA was not tested in this study.

The results obtained in cellular models of Huntington's disease outlined above prompted us to test whether transcriptional downregulation also occurs in the brains of subjects with Huntington's disease using archival transcriptome data[40,41]. We applied gene set analysis to calculate group mean change, which allows comparison of many control and subject samples[42]. SITA-target genes identified from HEK293 showed a robust downregulation in subject brain samples as compared to healthy controls (Fig. 5g). These included genes encoding metabolic enzymes of the lower glycolytic pathway that were transcriptionally downregulated upon heat shock in a NELFE-dependent manner (Fig. 5h, Supplementary Fig. 4a–c and Supplementary Fig. 10f,g). Taken together with the SITA manifestations in the cellular model of HTT (Fig. 5e,f and Supplementary Fig. 10a–e), the analyses of HTT subject brain transcriptomes suggest that brains may evoke SITA.

Discussion

In this study we present a molecular pathway that mediates SITA caused by heat shock as a stress model. We report three mechanistic steps leading to SITA. First, N-TEFs increase at promoters of SITA target genes. Second, p38 kinase translocates from the cytosol to the nucleus and binds promoters of downregulated genes, causing an increase of N-TEFs at these promoters upon heat shock. Third, active translation and protein ubiquitination are required for heat shock–induced SITA. Notably, proteins that are actively translated during heat shock are subjected to ubiquitination, linking translation and ubiquitination with transcriptional response to stress.

The biochemical basis of increased N-TEFs at chromatin during stress is not clear. All the subunits of the NELF complex are SUMOylated during heat shock (based on our analysis of data in ref. [43]). This post-translational modification is thought to act like 'glue'[44,45], probably increasing the residence time of N-TEFs at chromatin to enable SITA. In this context, how different N-TEFs cooperate with each other, either in a gene-dependent manner or globally, and how such interactions operate during recovery from stress will be critical to understand. Whether the NTEF-dependent transcriptional downregulation reported here is coordinated with HSF-driven chaperone upregulation will be an important question to address. Stress signaling among p38, HSF and N-TEFs may hold clues about coordination among different branches of the stress response.

We identified the p38 signaling module as a key link between active translation and nuclear gene regulation. How the same signaling cascade is repurposed under different stress conditions such as DNA damage[34,35,46] will be an area of future investigation. Our study describes the genomic targets of p38 kinase for the first time in mammalian cells exposed to proteotoxic stress. How p38 is activated by stress, how it gets recruited to specific loci and how it reorganizes transcriptional regulators at promoters is not understood. Notably, p38 kinase is activated in striatal neurons of R6/2 mouse models of Huntington's disease, suggesting p38 as a possible therapeutic target for neurodegeneration[47,48].

The stress response to proteostasis imbalance in the cytosol or endoplasmic reticulum is characterized by not only transcriptional changes, but also translational arrest, reducing protein synthesis from most cellular mRNA[49]. Inactivation of eukaryotic translation initiation factor (eIF1α) has a critical role in translational arrest after stress[50]. The N-TEF-dependent transcriptional downregulation reported here probably coordinates with translational arrest under stress in at least three independent ways. First, SITA reduces fresh mRNA abundance, thus decreasing ribosomal load during stress. Second, nascent transcription of the gene encoding eIF1α is downregulated, contributing to inactivation of these two key translational regulators upon stress. Finally, integrating nascent-chain ubiquitination with the transcriptional stress response, as shown here, establishes a sophisticated feedback system between transcription and translational flux. A critical next step will be to identify E3 ubiquitin ligase(s) involved in ubiquitination of nascent chains upon heat shock.

Our results suggest that the chronic stress of protein misfolding in the context of neurodegeneration may lead to recruitment of N-TEFs at chromatin and concomitant transcriptional downregulation. Whether nascent proteins are ubiquitinated in neurodegenerative brains of subjects with Huntington's disease warrants further investigation. Such gene downregulation probably reduces the burden on protein folding machinery during stress, giving cells an opportunity to recover from misfolding. Mutation in any component of the pathway leading to gene downregulation under stress would exacerbate disease progression. Thus our work provides the mechanistic basis of stress-induced transcriptional downregulation, with wide ramifications for the medical field that pave new avenues of possible therapeutic intervention.

Online content

Any methods, additional references, Nature Research reporting summaries, source data, statements of data availability and associated accession codes are available at https://doi.org/10.1038/s41594-018-0182-x.

Received: 29 March 2018; Accepted: 21 December 2018;
Published online: 4 February 2019

References

1. Morimoto, R. I. Regulation of the heat shock transcriptional response: cross talk between a family of heat shock factors, molecular chaperones, and negative regulators. *Genes Dev.* **12**, 3788–3796 (1998).
2. Akerfelt, M., Morimoto, R. I. & Sistonen, L. Heat shock factors: integrators of cell stress, development and lifespan. *Nat. Rev. Mol. Cell Biol.* **11**, 545–555 (2010).
3. Gomez-Pastor, R., Burchfiel, E. T. & Thiele, D. J. Regulation of heat shock transcription factors and their roles in physiology and disease. *Nat. Rev. Mol. Cell Biol.* **19**, 4–19 (2018).

4. Li, J., Labbadia, J. & Morimoto, R. I. Rethinking HSF1 in stress, development, and organismal health. *Trends. Cell Biol.* **27**, 895–905 (2017).
5. Spradling, A., Penman, S. & Pardue, M. L. Analysis of drosophila mRNA by in situ hybridization: sequences transcribed in normal and heat shocked cultured cells. *Cell* **4**, 395–404 (1975).
6. Jamrich, M., Greenleaf, A. L. & Bautz, E. K. Localization of RNA polymerase in polytene chromosomes of Drosophila melanogaster. *Proc. Natl Acad. Sci. USA* **74**, 2079–2083 (1977).
7. Mahat, D. B., Salamanca, H. H., Duarte, F. M., Danko, C. G. & Lis, J. T. Mammalian heat shock response and mechanisms underlying its genome-wide transcriptional regulation. *Mol. Cell* **62**, 63–78 (2016).
8. Gasch, A. P. et al. Genomic expression programs in the response of yeast cells to environmental changes. *Mol. Biol. Cell.* **11**, 4241–4257 (2000).
9. Duarte, F. M. et al. Transcription factors GAF and HSF act at distinct regulatory steps to modulate stress-induced gene activation. *Genes Dev.* **30**, 1731–1746 (2016).
10. Vihervaara, A. et al. Transcriptional response to stress is pre-wired by promoter and enhancer architecture. *Nat. Commun.* **8**, 255 (2017).
11. Core, L. J. & Lis, J. T. Transcription regulation through promoter-proximal pausing of RNA polymerase II. *Science* **319**, 1791–1792 (2008).
12. Adelman, K. & Lis, J. T. Promoter-proximal pausing of RNA polymerase II: emerging roles in metazoans. *Nat. Rev. Genet.* **13**, 720–731 (2012).
13. Kwak, H. & Lis, J. T. Control of transcriptional elongation. *Annu. Rev. Genet.* **47**, 483–508 (2013).
14. Bunch, H. et al. TRIM28 regulates RNA polymerase II promoter-proximal pausing and pause release. *Nat. Struct. Mol. Biol.* **21**, 876–883 (2014).
15. Stadelmayer, B. et al. Integrator complex regulates NELF-mediated RNA polymerase II pause/release and processivity at coding genes. *Nat. Commun.* **5**, 5531 (2014).
16. Chen, F. X. et al. PAF1, a molecular regulator of promoter-proximal pausing by rna polymerase II. *Cell* **162**, 1003–1015 (2015).
17. Paparidis, N. F., Durvale, M. C. & Canduri, F. The emerging picture of CDK9/P-TEFb: more than 20 years of advances since PITALRE. *Mol. Biosyst.* **13**, 246–276 (2017).
18. Kwak, H., Fuda, N. J., Core, L. J. & Lis, J. T. Precise maps of RNA polymerase reveal how promoters direct initiation and pausing. *Science* **339**, 950–953 (2013).
19. Palozola, K. C. et al. Mitotic transcription and waves of gene reactivation during mitotic exit. *Science* **358**, 119–122 (2017).
20. Ong, S. E. et al. Stable isotope labeling by amino acids in cell culture, SILAC, as a simple and accurate approach to expression proteomics. *Mol. Cell. Proteomics* **1**, 376–386 (2002).
21. Gilchrist, D. A. et al. NELF-mediated stalling of Pol II can enhance gene expression by blocking promoter-proximal nucleosome assembly. *Genes Dev.* **22**, 1921–1933 (2008).
22. Chen, F. X. et al. PAF1 regulation of promoter-proximal pause release via enhancer activation. *Science* **357**, 1294–1298 (2017).
23. Court, S. J., Waclaw, B. & Allen, R. J. Lower glycolysis carries a higher flux than any biochemically possible alternative. *Nat. Commun.* **6**, 8427 (2015).
24. Bersuker, K., Brandeis, M. & Kopito, R. R. Protein misfolding specifies recruitment to cytoplasmic inclusion bodies. *J. Cell Biol.* **213**, 229–241 (2016).
25. Santagata, S. et al. Tight coordination of protein translation and HSF1 activation supports the anabolic malignant state. *Science* **341**, 1238303 (2013).
26. Salomons, F. A. et al. Selective accumulation of aggregation-prone proteasome substrates in response to proteotoxic stress. *Mol. Cell. Biol.* **29**, 1774–1785 (2009).
27. Xu, G. et al. Vulnerability of newly synthesized proteins to proteostasis stress. *J. Cell Sci.* **129**, 1892–1901 (2016).
28. Hanna, J., Leggett, D. S. & Finley, D. Ubiquitin depletion as a key mediator of toxicity by translational inhibitors. *Mol. Cell. Biol.* **23**, 9251–9261 (2003).
29. Abravaya, K., Phillips, B. & Morimoto, R. I. Attenuation of the heat shock response in HeLa cells is mediated by the release of bound heat shock transcription factor and is modulated by changes in growth and in heat shock temperatures. *Genes Dev.* **5**, 2117–2127 (1991).
30. Duttler, S., Pechmann, S. & Frydman, J. Principles of cotranslational ubiquitination and quality control at the ribosome. *Mol. Cell* **50**, 379–393 (2013).
31. Wang, F., Durfee, L. A. & Huibregtse, J. M. A cotranslational ubiquitination pathway for quality control of misfolded proteins. *Mol. Cell* **50**, 368–378 (2013).
32. Cuadrado, A. & Nebreda, A. R. Mechanisms and functions of p38 MAPK signalling. *Biochem. J.* **429**, 403–417 (2010).
33. Davis, R. J. Signal transduction by the JNK group of MAP kinases. *Cell* **103**, 239–252 (2000).
34. Hotamisligil, G. S. & Davis, R. J. Cell signaling and stress responses. *Cold Spring Harb. Perspect. Biol.* **8**, a006072 (2016).
35. Wood, C. D., Thornton, T. M., Sabio, G., Davis, R. A. & Rincon, M. Nuclear localization of p38 MAPK in response to DNA damage. *Int. J. Biol. Sci.* **5**, 428–437 (2009).
36. de Nadal, E., Ammerer, G. & Posas, F. Controlling gene expression in response to stress. *Nat. Rev. Genet.* **12**, 833–845 (2011).
37. Young, P. R. et al. Pyridinyl imidazole inhibitors of p38 mitogen-activated protein kinase bind in the ATP site. *J. Biol. Chem.* **272**, 12116–12121 (1997).
38. Tatham, M. H., Matic, I., Mann, M. & Hay, R. T. Comparative proteomic analysis identifies a role for SUMO in protein quality control. *Sci. Signal.* **4**, rs4 (2011).
39. Hageman, J. et al. A DNAJB chaperone subfamily with HDAC-dependent activities suppresses toxic protein aggregation. *Mol. Cell* **37**, 355–369 (2010).
40. Brehme, M. et al. A chaperome subnetwork safeguards proteostasis in aging and neurodegenerative disease. *Cell Rep.* **9**, 1135–1150 (2014).
41. Hodges, A. et al. Regional and cellular gene expression changes in human Huntington's disease brain. *Hum. Mol. Genet.* **15**, 965–977 (2006).
42. Hadizadeh Esfahani, A., Sverchkova, A., Saez-Rodriguez, J., Schuppert, A. A. & Brehme, M. A systematic atlas of chaperome deregulation topologies across the human cancer landscape. *PLoS Comput. Biol.* **14**, e1005890 (2018).
43. Niskanen, E. A. et al. Global SUMOylation on active chromatin is an acute heat stress response restricting transcription. *Genome Biol.* **16**, 1–19 (2015).
44. Matunis, M. J., Zhang, X. D. & Ellis, N. A. SUMO: the glue that binds. *Dev. Cell* **11**, 596–597 (2006).
45. Niskanen, E. A. & Palvimo, J. J. Chromatin SUMOylation in heat stress: to protect, pause and organise?: SUMO stress response on chromatin. *Bioessays*. https://doi.org/10.1002/bies.201600263 (2017).
46. Borisova, M. E. et al. p38-MK2 signaling axis regulates RNA metabolism after UV-light-induced DNA damage. *Nat. Commun.* **9**, 1017 (2018).
47. Gianfriddo, M., Melani, A., Turchi, D., Giovannini, M. G. & Pedata, F. Adenosine and glutamate extracellular concentrations and mitogen-activated protein kinases in the striatum of Huntington transgenic mice. Selective antagonism of adenosine A2A receptors reduces transmitter outflow. *Neurobiol. Dis.* **17**, 77–88 (2004).
48. Taylor, D. M. et al. MAP kinase phosphatase 1 (MKP-1/DUSP1) is neuroprotective in Huntington's disease via additive effects of JNK and p38 inhibition. *J. Neurosci.* **33**, 2313–2325 (2013).
49. Shalgi, R. et al. Widespread regulation of translation by elongation pausing in heat shock. *Mol. Cell* **49**, 439–452 (2013).
50. Pavitt, G. D. & Ron, D. New insights into translational regulation in the endoplasmic reticulum unfolded protein response. *Cold Spring Harb. Perspect. Biol.* **4**, a012278 (2012).

Acknowledgements

We thank Y.L. Dréan (University of Rennes), H. Kampinga (University of Groningen), R. Kopito (Stanford University), J.T. Lis (Cornell University), R. Paro (ETH), A. Shilatifard (Northwestern University), L. Sistonen (University of Turku), E. Trompouki (Max Planck Institute of Immunobiology and Epigenetics) and U. Wölfle (University of Freiburg) for sharing cell lines, protocols and plasmids; and J. Büscher, G. Mittler and sequencing and bioinformatics facilities for data acquisition and help with the analyses. We acknowledge critical discussions with P. Beli, U. Hartl, J. Palvimo, L. Sistonen and colleagues at the Max Planck Institute of Immunobiology and Epigenetics. Excellent technical assistance from S. Bares and A. Antonova is acknowledged. R.S. acknowledges financial support by the Max Planck Society, the German Research Foundation through the collaborative research center Medical Epigenetics, through the research grant SA 3190 (R.S.) and through Germany's Excellence Strategy (CIBSS, EXC-2189, project ID 390939984).

Author contributions

R.S. conceived the project; R.S., F.A.G. and P.T. designed the study; F.A.G., P.T. and A.K. performed experiments and interpreted the results; F.A.G. conceived and performed experiments on nascent-protein ubiquitination during the revision process; B.H. performed all the computational analyses; F.A.G. and R.S. wrote the manuscript with input from all the authors.

Competing interests

The authors declare no competing interests.

Additional information

Supplementary information is available for this paper at https://doi.org/10.1038/s41594-018-0182-x.

Reprints and permissions information is available at www.nature.com/reprints.

Correspondence and requests for materials should be addressed to R.S.

Publisher's note: Springer Nature remains neutral with regard to jurisdictional claims in published maps and institutional affiliations.

Methods

Cell culture. Human cell lines HCT116 (obtained from A. Shilatifard, Northwestern University), HeLa and Flp-In T-Rex HEK293 (obtained from R. Paro, ETH Zürich) were cultured in DMEM high glucose (Sigma-Aldrich, D5671) supplemented with 10% FBS (Sigma-Aldrich, F7524). Human cell line K562 (obtained from E. Trompouki, Max Planck Institute for Immunobiology and Epigenetics) was cultured in IMDM (Gibco, 21980) supplemented with 10% FBS. Human cell line SH-SY5Y (obtained from U. Wölfle, Universitätsklinikum) was cultured in DMEM/F-12 (Gibco, 31330) supplemented with 15% FBS. Wild-type and HSF1-HSF2 double-knockout mouse embryonic fibroblasts were cultured in DMEM (obtained from Y. Le Dréan, Université de Rennes). All cell types were also supplemented with 2 mM L-glutamine (Sigma-Aldrich, G7513) and 1% penicillin-streptomycin (Sigma-Aldrich, P4333). Cells were kept at 37 °C in 5% CO_2. Cells were routinely tested for mycoplasma contamination by PCR.

Primary cultures. PBMCs were freshly isolated from venous blood of healthy male human donors with their consent. The Safety Department of Max Planck Institute of Immunobiology and Epigenetics approved the study protocol. Local regulations and ethical guidelines imposed by Max Planck Society were strictly followed while handling human blood. PBMCs were isolated by Percoll density-gradient centrifugation (Pan Biotech, P04-60500), according to the manufacturer's instructions. Cells were plated in 24-well culture plates. T cell blasts were generated by stimulation of PBMCs with 1.25 µg ml^{-1} phytohemagglutinin (Sigma-Aldrich, L1668) and 100 U ml^{-1} interleukin-2 (Peprotech, 200–02) for 5–7 d.

Heat shock treatment. Unless otherwise stated, heat shock treatment was done by moving tissue-culture plates with growing cells from an incubator at normal growth temperature (37 °C) into an incubator at heat-shock temperatures (43 °C) for 1.5 h. Heat-shock treatment of K562 cells was done for 0.5 h. Heat-shock treatment of HeLa cells was done at 42 °C for the indicated times for activation and attenuation phase experiments[29]. To explore whether different heat-shock paradigms could influence the results obtained, we also applied acute heat shock, as described[51]. Briefly, two plates were grown up to 80% confluence. Medium from one of the plates was removed, preheated to 43 °C and added to the other plate from which the medium was withdrawn. The plate was then placed at 43 °C for 1.5 h.

Plasmid transfection. HEK293 and SH-SY5Y cells were transfected with Lipofectamine 3000 (Life Technologies, L3000) according to the manufacturer's instructions. Q25_GFP HTT exon 1 and Q103_GFP HTT exon 1 plasmids (a kind gift from R. Kopito, Stanford University) were transiently transfected in HEK293 and SH-SY5Y. HDQ23-GFP-HIS and HDQ119-GFP-HIS (a gift from H. Kampinga, University of Groningen) were stably transfected in Flp-In T-Rex HEK293 grown in 100 µg ml^{-1} Zeocin (Invitrogen, R25001) for at least a week before transfection. Stable positive clones were selected for at least 2 weeks in 15 µg ml^{-1} blasticidin S (Carl Roth CP14.1) and 100 µg ml^{-1} hygromycin B (Thermo Fisher Scientific, 10687010). Expression of HTT protein variants was induced with 1 µg ml^{-1} tetracycline (Sigma-Aldrich, T7660).

Chemical treatments. A summary of all the chemicals used with information on catalog numbers, supplier, concentration and time of treatment is in Supplementary Table 2.

RNA interference. siRNA-based gene knockdown was performed using RNAiMAX (Invitrogen, 13778075) according to the manufacturer's instructions and SMARTpool siRNA reagent (Dharmacon). This reagent is a pool of four siRNA duplexes designed to target distinct sites within the specific gene of interest, and shown in silico not to have significant off-target effects. Cherry-pick libraries from Dharmacon comprising several siRNA SMARTpool and nontargeting controls were ordered. HEK293 cells were plated 16 h before transfection. SMARTpool siRNAs were transfected at 20 nM. Cells were further incubated for 48 h before being harvested for analysis. Knockdown efficiency was confirmed by western blotting. A list of all oligonucleotides used is in Supplementary Table 3.

Cellular fractionation and chromatin extraction. Total cell extracts for western blot analysis were obtained by PBS wash and cell lysis in lysis buffer (50 mM Tris-HCl, pH 6.8, 2% SDS and 10% glycerol). Chromatin extraction was done as described with minor modifications[52]. Briefly, cells were washed twice with ice-cold PBS and an aliquot was taken out and saved as total cell extract. Remaining cells were resuspended in buffer A (10 mM HEPES, pH 7.9, 5 mM $MgCl_2$, 0.25 M sucrose) and incubated on ice for 8 min. Cells were passed through 18 G needles ten times and centrifuged at 2,000*g* for 10 min at 4 °C. The nuclear pellet was washed with buffer A, resuspended in 0.5 M buffer B (20 mM HEPES, pH 7.9, 0.5 M KCl, 1.5 mM $MgCl_2$, 0.1 mM EDTA, 10% glycerol) and incubated on a rocker for 30 min at 4 °C. The suspension was centrifuged and the chromatin pellet was resuspended in 2 M buffer B (20 mM HEPES, pH 7.9, 2 M KCl, 1.5 mM $MgCl_2$, 0.1 mM EDTA, 10% glycerol), passed through a 200-µl cut tip ten times and incubated while rocking for 30 min at 4 °C. Chromatin fractions were sonicated for 15 cycles (30 s on, 30 s off, high power) in Bioruptor. Samples were centrifuged at 20,000*g* for 30 min to remove debris and unsonicated material.

Other methods of chromatin extraction as shown in Supplementary Fig. 3c–e were followed according to their original reports[53–55].

Stable isotope labeling with amino acids in cell culture. SILAC was done as described[20]. Briefly, amino acids containing different isotopes of certain atoms were used to label proteins in cell culture. HEK293 cells were cultured in medium lacking arginine and lysine but supplemented either with [$^{13}C_6$]L-arginine and [$^2H_4$]L-lysine (heavy) or with unlabeled versions of L-arginine and L-lysine (light). To avoid contamination of medium with unlabeled amino acids, dialyzed FBS was used. In addition, the labeling was started from an unlabeled culture with <1% of the final cell number. The labeling procedure was carried out for at least five cell divisions before amplifying cells for the experiments. HEK293 cells grown in different labeled isotopes were either exposed to control (37 °C) or heat-shock conditions (43 °C, 1.5 h). Cells were pooled and fractionated and chromatin fractions were obtained using 2 M KCl salt extraction as described above. The resulting samples were separated by SDS–polyacrylamide gel electrophoresis (NuPAGE 4–12%) and subjected to in-gel digestion followed by nano-LC-MS analysis on an Agilent1200 nanoHPLC system interfaced with a Thermo Fisher OrbitrapXL ETD mass spectrometer. Experiments were done in triplicate. The replicates were generated using the label-swap strategy (that is, light labeling was assigned to control sample in one replicate but to heat-shock sample in the next, and vice versa for the heavy labeling).

Protein complex enrichment. The online tool COMPLEAT was used to search for enrichment of protein complexes[56] (http://www.flyrnai.org/compleat/). The data in Supplementary Data Set 4 was used as input. The option parameters were set as follows: $P = 10^{-3}$; complex size, 3–20 proteins; random sample size, 1,000. Only literature complexes from the output were used for further analysis. The output is in Supplementary Table 1.

Chromatin immunoprecipitation (quantitative PCR and sequencing). Chromatin was extracted and sheared as described[57]. Briefly, cells were fixed using 1% methanol-free formaldehyde (Thermo Scientific, 28906) in DMEM (HEK293) or IMDM (K562) at room temperature for 10 min, followed by 5 min blocking in 0.125 M glycine. Cells were washed twice with ice-cold PBS. The cell pellet was resuspended in Farnham buffer (5 mM PIPES, pH 8; 85 mM KCl; 0.5% Igepal). Cell suspensions were sonicated in 1 ml Covaris tubes (Covaris, 520130) using Covaris S220 with the following settings: peak power = 75; duty factor = 2; cycles/burst = 200. Sonication time varied from cell type to cell type; K562 = ~2.5 min and HEK293 = ~3 min. Isolated nuclei were washed with Farnham buffer and suspended in shearing buffer (10 mM Tris-HCl, pH 8; 0.1% SDS; 1 mM EDTA). Chromatin was sheared by sonication in 1-ml Covaris tubes using the following settings: peak power = 140; duty factor = 5; cycles/burst = 200, time = 25–30 min. Debris was removed by centrifugation. A DNA fragment–size distribution of 200–600 bp was considered as ideal chromatin for ChIP. Chromatin was diluted 1:1 with IP buffer (10 mM Tris-HCl, pH 8; 100 mM NaCl, 1 mM EDTA, 0.5 mM EGTA, 0.1% sodium deoxicholate, 0.1% *N*-lauroylsarcosine) to achieve a final 0.05% SDS concentration. Good quality chromatin (200 µg) was used for immunoprecipitation as described[58]. Briefly, Protein A or G magnetic beads (Life Technologies, 10002D and 10004D, respectively) were incubated (rotated) with 5–10 µg of antibody for 6 h at 4 °C. This bead–antibody complex was then incubated overnight at 4 °C with chromatin. As one normalization method for RNA Pol II ChIP-Seq, mouse chromatin was used according to the spike-in method described[59]. Briefly, mouse chromatin from embryonic stem cells was independently crosslinked and sheared to obtain the same size distribution as in human chromatin used in all experiments, and then aliquoted and stored. When required, this control chromatin was mixed with chromatin from treated human cells at a 2.5:97.5 ratio and immunoprecipitation was performed. A list of all antibodies used in this study is in Supplementary Table 4.

An aliquot of chromatin (containing mouse spike-in chromatin) was saved as input DNA. Beads were washed and DNA–protein complexes were eluted from the beads by heating at 65 °C in elution buffer (50 mM Tris-HCl, pH 8.0, 10 mM EDTA and 1% SDS). Crosslinking was reversed for 6 h at 70 °C and samples were treated with 200 µg ml^{-1} RNase A (Applichem, A3832) and 200 µg ml^{-1} proteinase K (Sigma-Aldrich, P2308). ChIP DNA was purified with phenol–chloroform extraction and ethanol precipitation and used either for ChIP-qPCR or library preparation for next-generation sequencing. For ChIP-qPCR, enrichment of the immunoprecipitated DNA at the corresponding loci was expressed as a percentage relative to the input DNA.

For ChIP-seq, DNA libraries were prepared from immunoprecipitated DNA. Sequencing libraries were prepared using the NEBNext Ultra II DNA Library Prep kit for Illumina (NEB E7645S). Some 2–5 ng of immunoprecipitated DNA was used for library preparation. Library size distribution was monitored by capillary electrophoresis (Agilent 2100 Bioanalyzer, High Sensitivity DNA Chips (Agilent, 5067–4626)). Libraries were sequenced paired-end on HiSeq 2500, HiSeq 3000 or NextSeq 500 instruments (Illumina). For each experiment, at least two biological replicates were generated and sequenced with a minimum depth of 10 million in the case of NELF immunoprecipitation and 40 million for RNA Pol II immunoprecipitation.

Chromatin immunoprecipitation sequencing analysis. ChIP-seq reads were aligned to the human genome build hg38 using Bowtie2[60]. Duplicate and discordant reads were removed. Peak calling was done with MACS2[61] (model-based analysis of ChIP-seq) using "–keep-dup all," "–nomodel," "–extsize" and "–broad." Gene annotations and TSS information for human genes were taken from Gencode annotation release 26. Genes considered for differential gene body reads per kilobase per million fragments mapped analysis were filtered similarly as described[16]: RNA Pol II peaks ($P < 1 \times 10^{-5}$) had to overlap the TSS (from the TSS to 500 bp downstream of the TSS), the reads per million (RPM) of the same region had to be at least 1, and genes had to be >2 kb long and >1 kb distant to any neighboring gene. If a gene had several TSSs, the highest occupied (based on RPM) was taken. Gene body was defined for the remaining genes as TSS + 1,500 bp to transcription end site (TES) – 500 bp. Reads overlapping the gene body regions were counted using bedtools[62]. Differential gene expression was done using DESeq2[63]. We compared three independent normalization methods for RNA Pol II ChIP-seq analysis: (1) based on sequencing depth; (2) using the 3′ end of long genes as described[7]; and (3) with a spike-in method as described[59]. Similar results were obtained when comparing these three normalization methods, except for the final number of differentially expressed genes. For visualization, the paired-end reads were extended to fragment size and normalized to total reads aligned (RPM) using deeptools2[64]. MAplots were generated with ggplot2[65], with the *x*-axis representing the mean of NHS gene body fragments per kilobase of transcript per million mapped reads. Heatmaps were generated with gplots package[66] after batch effect removal using limma package[67], and profile plots were generated with deeptools2[64]. Violin plots were generated with the vioplot package in R[68] using the ratio of the gene body counts. Pausing index was computed for the top downregulated genes as the ratio of RNA Pol II ChIP-seq coverage at promoter over coverage at gene body. The promoter and gene body region were defined as described above. We used the maximum coverage for the promoters and the median coverage for the gene body. NELF ChIP-seq ratio for all downregulated genes was calculated as the ratio of the coverage at promoter (TSS ± 500 bp) in heat-shocked samples over non-heat-shocked samples. All browser tracks were visualized using Integrative Genome Viewer (http://software.broadinstitute.org/software/igv/).

Precision nuclear run-on sequencing. Precision nuclear run-on sequencing (PRO-seq) was done as described[69]. Briefly, 10×10^6 HEK293 cells were used for each PRO-seq experiment. Cells were harvested and permeabilized. A 2-biotin label run-on reaction was done to label nascently transcribed RNA. A 2× nuclear run-on mix was mixed with biotin-labeled CTP and UTP. The nuclear run-on reaction was carried out for 3 min at 37 °C. The reaction was stopped by adding Trizol LS (Ambion, 10296028) followed by vigorous vortexing. RNA was isolated by standard procedure. Nascently transcribed RNA was fragmented by base hydrolysis (NaOH) leading to 100-bp RNA suitable for sequencing. Streptavidin-coated magnetic beads were used to enrich for biotin-labeled RNA using affinity purification. RNA was mixed with prewashed streptavidin beads and incubated at room temperature. Beads were washed and resuspended in Trizol and RNA was isolated. A 3′ RNA adaptor (VRA3-5uM) was ligated at the 3′ end of biotin-labeled nascent RNA using ligation mix (T4 RNA ligase buffer, 1 mM ATP, 10% PEG, RNase inhibitor, T4 RNA ligase I). A second biotin-RNA enrichment was done to enrich for labeled nascent RNA and remove unligated adaptors. The 5′ OH generated by base hydrolysis was then converted to 5′ phosphate by treatment with T4 polynucleotide kinase. A 5′ RNA adaptor (VRA5) was ligated at the 5′ end of RNA using the ligation mix described previously. A third round of enrichment was done to enrich for labeled RNA and remove any unligated adaptors. Nascent RNA was then reverse transcribed using RP1 and RTP reverse transcription primers (2.5 μM each). A test PCR amplification was then done to determine number of PCR cycles for amplification. A PCR cycle that gave sufficient amount of product, no overamplification and 50–75% of unused primers was considered optimal and used for final amplification. Full-scale PCR amplification was done using the following PCR mix (1× HF buffer, 1 M betaine, 250 μM dNTP mix, 250 nM RP1 primer, 250 nM RP1-n primer, 0.04 units μl^{-1} Phusion DNA polymerase). PCR-amplified DNA was then size selected (150–350 bp) by polyacrylamide gel electrophoresis purification with some modifications from the original protocol[69]. DNA was then extracted using phenol-chloroform extraction. DNA pellet was redissolved in nuclease-free water and DNA library size distribution was monitored by capillary electrophoresis. Libraries were sequenced single-end on a HiSeq 3000 instrument (Illumina).

Precision nuclear run-on sequencing analysis. PRO-seq data analysis was done as described[69] with slight modifications. Briefly, Cutadapt was used to cut adaptor from sequenced reads. Filtered reads were first mapped to a single copy of ribosomal DNA to remove the contribution of nascent RNAs from ribosomal genes. The remaining reads were mapped to human genome build hg38 using Bowtie2[60] using default parameters. PRO-seq libraries were normalized using the 3′ end of long genes. DESeq2[63] was used to identify genes with differential PRO-seq density between non-heat-shocked and heat-shocked libraries. Heatmaps were generated with gplots package[66] after batch effect removal using limma package[67].

Quantitative PCR with reverse transcription and nascent-transcript quantification assay. RNA was isolated after TRIzol extraction (Sigma-Aldrich, T9424). RNA samples were treated with DNAse for 1 h (Life Technologies, AM1907) and first-strand cDNA was synthesized (Thermo Fisher Scientific, K1612) according to the manufacturer's instructions. Nascent transcripts were detected using intron-exon primer pairs as described[19]. We selected genes to quantify based on RNA Pol II ChIP-seq data (Supplementary Fig. 1). cDNA was amplified in a Step One Plus Real-Time PCR system (Applied Biosystems) using SYBRgreen (Thermo Fisher Scientific, AB-1163). DNA amounts were quantified using the ΔΔCt method, and the nontreated condition was set to 1. A list of all primers used is in Supplementary Table 3.

Metabolic labeling of newly translated proteins. Newly synthesized proteins were labeled, purified and detected using the BONCAT technique[70]. Briefly, 1–2 million cells were starved of methionine by 1 h of growth in methionine-free medium (AthenaES, 420). For canavanine experiments, cells were either incubated in arginine-containing medium or 1 mM canavanine (Sigma-Aldrich, C9758) for 2 h. Cells were then incubated with the azide-bearing artificial amino acid L-azidohomoalanine, a methionine analog (AHA; Invitrogen, C10102) for the indicated times and lysed in lysis buffer (50 mM Tris-HCl, pH 8, 1% SDS). Proteins labeled with the AHA amino acid were biotinylated by click-chemistry reactions. Biotin-PEG4-alkyne (Sigma-Aldrich, 764213) and the Click-iT Protein Reaction Buffer kit (Invitrogen, C10276) were used according to the manufacturer's instructions. Briefly, click reactions were performed with at least 20 μg protein extract and 400 μM final concentration of the alkyne for 20 min at 20 °C with strong shaking. Proteins were precipitated in methanol, resuspended and either subjected to western blot or to biotin purification to separate newly translated proteins from the rest. Biotin purifications were performed using Dynabeads MyOne Streptavidin C1 (Invitrogen, 65001) according to the manufacturer's instructions at room temperature for 20 min with gentle rotation. After purification, the flow through was collected and protein precipitated, and the beads were washed and boiled in loading buffer for western blot. For detection of biotinylated proteins, a streptavidin-horseradish peroxidase reagent was used (Thermo Fisher Scientific, 21130) at 1:10,000 dilution.

Polysome isolation. Total polysomes were isolated by ultracentrifugation in sucrose cushions as described[31]. Briefly, HEK293 cells in 15-cm dishes were lysed after heat shock or L-canavanine treatments in 2 ml of high-salt polysome lysis buffer (100 mM Tris, pH 7.4, 50 mM KCl, 25 mM $MgCl_2$, 100 $\mu g\,ml^{-1}$ cycloheximide, 100 μM PMSF, 5 mM *N*-ethylmaleimide, 20 $U\,ml^{-1}$ RNase OUT RNase inhibitor (Invitrogen) and 1% Triton X-100). Lysates were clarified by centrifugation and loaded on a 1.2-ml 35% sucrose cushion (in 10 mM Tris, pH 7.4, 85 mM KCl and 5 mM $MgCl_2$) and centrifuged for 1.5 h at 300,000*g* in a Beckman TLA-110 rotor at 4 °C. The supernatant was recovered and subjected to protein precipitation with methanol and chloroform. The sucrose cushion was discarded and the ribosome-containing pellet was resuspended in 200 μl polysome buffer (10 mM Tris, pH 7.4, 10 mM NaCl, 3 mM $MgCl_2$ and 0.2 mM dithiothreitol) and stored at −80 °C.

In vitro puromycin assays. Biotin-puromycin conjugation assays were performed as described[31]. Briefly, the following conditions were used: 10 mM Tris, pH 7.4, 400 mM KCl, 3 mM $MgCl_2$, 4 μM biotin-linked puromycin (Jena Bioscience, NU-925-BIO-S) and two A_{260} units of polysomes obtained as previously described[31] per 100-μl reaction. Puromycinylation reactions were performed for 1.5 h at 37 °C. After reaction, a 10% fraction was kept as input, and biotinylated polypeptides were purified using Dynabeads MyOne Streptavidin C1 (Invitrogen, 65001) according to the manufacturer's instructions at room temperature for 20 min with gentle rotation. After purification, the flow through was collected and protein precipitated, and the beads were washed and boiled in loading buffer for western blot. For detection of biotinylated proteins, a streptavidin-horseradish peroxidase reagent was used (Thermo Fisher Scientific, 21130) at 1:10,000 dilution.

Metabolite quantification. For quantification of cellular metabolites, HEK293 cells were grown in their normal growth medium. Metabolites were extracted from 1–2 million cells in extraction solution (methanol/water, 80:20). A fraction of this supernatant was used for targeted metabolomics in liquid chromatography followed by triple-quadrupole mass spectrometry (LC-QQQ-MS). Blank samples were used for adjusting background levels and spike-in samples with known metabolite composition to properly assign metabolite identities. Data were analyzed with MassHunter Quant software (Agilent).

Analysis of gene expression data from Huntington's disease cohorts. The data reported in Hodges et al. 2016 (ref. [41]) were used to compare gene expression in brain tissues from Huntington's disease and control samples. Genes significantly upregulated and downregulated in HEK293 cells upon heat shock were used (Supplementary Data Set 1) to identify the subset of genes that were also expressed in control brain samples (normalized expression value >500). We applied gene set analysis[71] to calculate group mean change, which allows comparison of many control and subject samples, as has been done recently[42].

Statistics. The Wilcoxon rank-sum test was used for Figs. 1g, 2e and 3d. The Student's *t*-test was used for Fig. 5h and Supplementary Fig. 10f,g.

Reporting Summary. Further information on research design is available in the Nature Research Reporting Summary linked to this article.

Data availability

All the deep-sequencing data reported in this study are deposited in Gene Expression Omnibus and are available under accession number GSE112379. The mass spectrometry proteomics data have been deposited with the ProteomeXchange Consortium via the PRIDE partner repository with the data set identifier PXD012077. The source data for Figs. 2d, 3c, 4g and 5c,f are available online. Uncropped images of Figs. 1c,d, 2a–c, 3a,b,f–j, 4b,c,f and 5a,b,e are available with the paper online. All other data will be made available upon request.

References

51. Mahat, D. B. & Lis, J. T. Use of conditioned media is critical for studies of regulation in response to rapid heat shock. *Cell Stress Chaperones* **22**, 155–162 (2017).
52. Margueron, R. et al. Ezh1 and Ezh2 maintain repressive chromatin through different mechanisms. *Mol. Cell* **32**, 503–518 (2008).
53. Henikoff, S., Henikoff, J. G., Sakai, A., Loeb, G. B. & Ahmad, K. Genome-wide profiling of salt fractions maps physical properties of chromatin. *Genome Res.* **19**, 460–469 (2009).
54. Kustatscher, G., Wills, K. L., Furlan, C. & Rappsilber, J. Chromatin enrichment for proteomics. *Nat. Protoc.* **9**, 2090–2099 (2014).
55. Tresini, M. et al. The core spliceosome as target and effector of non-canonical ATM signalling. *Nature* **523**, 53–58 (2015).
56. Vinayagam, A. et al. Protein complex-based analysis framework for high-throughput data sets. *Sci. Signal.* **6**, rs5 (2013).
57. Arrigoni, L. et al. Standardizing chromatin research: a simple and universal method for ChIP-seq. *Nucleic Acids Res.* **44**, e67 (2016).
58. Lee, T. I., Johnstone, S. E. & Young, R. A. Chromatin immunoprecipitation and microarray-based analysis of protein location. *Nat. Protoc.* **1**, 729–748 (2006).
59. Bonhoure, N. et al. Quantifying ChIP-seq data: a spiking method providing an internal reference for sample-to-sample normalization. *Genome Res.* **24**, 1157–1168 (2014).
60. Langmead, B. & Salzberg, S. L. Fast gapped-read alignment with Bowtie 2. *Nat. Methods* **9**, 357–359 (2012).
61. Zhang, Y. et al. Model-based analysis of ChIP-Seq (MACS). *Genome Biol.* **9**, R137 (2008).
62. Quinlan, A. R. & Hall, I. M. BEDTools: a flexible suite of utilities for comparing genomic features. *Bioinformatics* **26**, 841–842 (2010).
63. Love, M. I., Huber, W. & Anders, S. Moderated estimation of fold change and dispersion for RNA-seq data with DESeq2. *Genome Biol.* **15**, 550 (2014).
64. Ramirez, F. et al. deepTools2: a next generation web server for deep-sequencing data analysis. *Nucleic Acids Res.* **44**, W160–W165 (2016).
65. H. Wickham. *ggplot2: Elegant Graphics for Data Analysis*. (Springer-Verlag New York, 2009).
66. Warnes, G. W. et al. *gplots: Various R programming tools for plotting data*. https://cran.r-project.org/web/packages/gplots/index.html (2016).
67. Ritchie, M. E. et al. limma powers differential expression analyses for RNA-sequencing and microarray studies. *Nucleic Acids Res.* **43**, e47 (2015).
68. Adler, D. *vioplot: Violin plot. R package version 0.2.* https://cran.r-project.org/web/packages/vioplot/index.html (2005).
69. Mahat, D. B. et al. Base-pair-resolution genome-wide mapping of active RNA polymerases using precision nuclear run-on (PRO-seq). *Nat. Protoc.* **11**, 1455–1476 (2016).
70. Dieterich, D. C. et al. Labeling, detection and identification of newly synthesized proteomes with bioorthogonal non-canonical amino-acid tagging. *Nat. Protoc.* **2**, 532–540 (2007).
71. Efron, B. & Tibshirani, R. On testing the significance of sets of genes. *Ann. Appl. Stat.* **1**, 23 (2007).

nature research

Corresponding author(s): Ritwick Sawarkar

Reporting Summary

Nature Research wishes to improve the reproducibility of the work that we publish. This form provides structure for consistency and transparency in reporting. For further information on Nature Research policies, see Authors & Referees and the Editorial Policy Checklist.

Statistical parameters

When statistical analyses are reported, confirm that the following items are present in the relevant location (e.g. figure legend, table legend, main text, or Methods section).

n/a	Confirmed	
☐	☒	The exact sample size (*n*) for each experimental group/condition, given as a discrete number and unit of measurement
☐	☒	An indication of whether measurements were taken from distinct samples or whether the same sample was measured repeatedly
☐	☒	The statistical test(s) used AND whether they are one- or two-sided *Only common tests should be described solely by name; describe more complex techniques in the Methods section.*
☒	☐	A description of all covariates tested
☒	☐	A description of any assumptions or corrections, such as tests of normality and adjustment for multiple comparisons
☐	☒	A full description of the statistics including central tendency (e.g. means) or other basic estimates (e.g. regression coefficient) AND variation (e.g. standard deviation) or associated estimates of uncertainty (e.g. confidence intervals)
☐	☒	For null hypothesis testing, the test statistic (e.g. *F*, *t*, *r*) with confidence intervals, effect sizes, degrees of freedom and *P* value noted *Give P values as exact values whenever suitable.*
☒	☐	For Bayesian analysis, information on the choice of priors and Markov chain Monte Carlo settings
☒	☐	For hierarchical and complex designs, identification of the appropriate level for tests and full reporting of outcomes
☒	☐	Estimates of effect sizes (e.g. Cohen's *d*, Pearson's *r*), indicating how they were calculated
☐	☒	Clearly defined error bars *State explicitly what error bars represent (e.g. SD, SE, CI)*

Our web collection on statistics for biologists may be useful.

Software and code

Policy information about availability of computer code

Data collection	No custom software was used
Data analysis	No custom software was used

For manuscripts utilizing custom algorithms or software that are central to the research but not yet described in published literature, software must be made available to editors/reviewers upon request. We strongly encourage code deposition in a community repository (e.g. GitHub). See the Nature Research guidelines for submitting code & software for further information.

Data

Policy information about availability of data

All manuscripts must include a data availability statement. This statement should provide the following information, where applicable:

- Accession codes, unique identifiers, or web links for publicly available datasets
- A list of figures that have associated raw data
- A description of any restrictions on data availability

The following statement is already included in the Data Availability section in the Main text of the manuscript:
Data Availability
All the deep-sequencing data reported in this study are deposited in GEO and are available under accession number GSE112379. The mass spectrometry proteomics

data have been deposited to the ProteomeXchange Consortium via the PRIDE partner repository with the dataset identifier PXD012077. The source data for Figures 2D, 3C, 4G, 5C and 5F are available with the paper online. Uncropped images of Figures 1C-D, 2A-C, 3A-B, 3F-J, 4B-C,4F, 5A-B,5E are available with the paper online. All other data will be made available upon request.

Field-specific reporting

Please select the best fit for your research. If you are not sure, read the appropriate sections before making your selection.

☒ Life sciences ☐ Behavioural & social sciences ☐ Ecological, evolutionary & environmental sciences

For a reference copy of the document with all sections, see nature.com/authors/policies/ReportingSummary-flat.pdf

Life sciences study design

All studies must disclose on these points even when the disclosure is negative.

Sample size	Wherever applicable, detailed in Methods
Data exclusions	No data were excluded from the analysis.
Replication	All replication attempts were successful. Detailed in Methods.
Randomization	This study did not require randomization since it was carried out with experiments using cells in culture.
Blinding	Blinding was not carried out in this study. The authors consider that the study does not contain experiments where blinding would be applicable

Reporting for specific materials, systems and methods

Materials & experimental systems

n/a	Involved in the study
☒	☐ Unique biological materials
☐	☒ Antibodies
☐	☒ Eukaryotic cell lines
☒	☐ Palaeontology
☒	☐ Animals and other organisms
☐	☒ Human research participants

Methods

n/a	Involved in the study
☐	☒ ChIP-seq
☒	☐ Flow cytometry
☒	☐ MRI-based neuroimaging

Antibodies

Antibodies used	Antibodies used in this study are detailed in Supplementary Table 10.
Validation	All antibodies were employed following manufacturer's instructions.

Eukaryotic cell lines

Policy information about cell lines

Cell line source(s)	Stated in Methods.
Authentication	Cell lines authenticated by RNA-Seq (transcriptiome validation), where applicable. Data deposited in GEO as mentioned before.
Mycoplasma contamination	Cells routinely tested negative for Mycoplasma. Stated in Methods
Commonly misidentified lines (See ICLAC register)	---

Human research participants

Policy information about studies involving human research participants

Population characteristics	No population studies in this study.
Recruitment	Recruitment was performed by consent following institutional guidelines. Stated in Methods.

ChIP-seq

Data deposition

☒ Confirm that both raw and final processed data have been deposited in a public database such as GEO.

☒ Confirm that you have deposited or provided access to graph files (e.g. BED files) for the called peaks.

Data access links *May remain private before publication.*	The following statement is already included in the Data Availability section in the Main text of the manuscript: All the deep-sequencing data reported in this study are deposited in GEO and are available under accession number GSE112379. The data will be available for public upon acceptance of the manuscript.
Files in database submission	The following statement is already included in the Data Availability section in the Main text of the manuscript: All the deep-sequencing data reported in this study are deposited in GEO and are available under accession number GSE112379. The data will be available for public upon acceptance of the manuscript.
Genome browser session (e.g. UCSC)	The following statement is already included in the Data Availability section in the Main text of the manuscript: All the deep-sequencing data reported in this study are deposited in GEO and are available under accession number GSE112379. The data will be available for public upon acceptance of the manuscript.

Methodology

Replicates	Detailed in Methods
Sequencing depth	Detailed in Methods
Antibodies	Detailed in Supplementary Table 10
Peak calling parameters	Detailed in Methods
Data quality	Detailed in Methods
Software	Detailed in Methods